

Review

Efficient Planar Perovskite Solar Cells with ZnO Electron Transport Layer

Chufeng Qiu ^{1,2}, Yan Wu ^{1,2}, Jiaxing Song ^{2,3,*}, Wentao Wang ¹ and Zaifang Li ^{2,4,*}

¹ School of Materials Science and Engineering, Zhejiang Sci-Tech University, Hangzhou 310018, China

² China-Australia Institute for Advanced Materials and Manufacturing, Jiaxing University, Jiaxing 314001, China

³ R&D Centre, JinkoSolar, Haining 314416, China

⁴ Nanotechnology Research Institute (NRI), Jiaxing University, Jiaxing 314001, China

* Correspondence: songjx@zjxu.edu.cn (J.S.); zaifang.li@zjxu.edu.cn (Z.L.)

Abstract: Perovskite solar cells (PSCs) have experienced rapid development in the past period of time, and a record efficiency of up to 25.7% has been yielded. At present, the PSCs with the planar structure are the most prevailing, which not only can significantly simplify the device fabrication process but also reduce the processing temperature. Particularly, the electron transport layer (ETL) plays a critical role in boosting the device performance of planar PSCs. ZnO is a promising candidate as the ETL owing to its high transparency, suitable energy band structure, and high electron mobility. Moreover, ZnO is easy to be processed at a low cost and low energy. This review mainly summarized the recent advances in the application and strategic optimization of ZnO ETL for planar PSCs. The basic properties of ZnO, including energy levels, mobility, processability, trap defects, as well as chemical stability, are clearly clarified. The most available deposition means for preparing ZnO ETLs were also described briefly. Finally, we presented the challenges and guidelines for utilizing ZnO as ETL on efficient planar PSCs.

Keywords: ZnO; electron transport layer; perovskite solar cell; planar structure



Citation: Qiu, C.; Wu, Y.; Song, J.; Wang, W.; Li, Z. Efficient Planar Perovskite Solar Cells with ZnO Electron Transport Layer. *Coatings* **2022**, *12*, 1981. <https://doi.org/10.3390/coatings12121981>

Academic Editor: Alessandro Latini

Received: 7 November 2022

Accepted: 15 December 2022

Published: 17 December 2022

Publisher's Note: MDPI stays neutral with regard to jurisdictional claims in published maps and institutional affiliations.



Copyright: © 2022 by the authors. Licensee MDPI, Basel, Switzerland. This article is an open access article distributed under the terms and conditions of the Creative Commons Attribution (CC BY) license (<https://creativecommons.org/licenses/by/4.0/>).

1. Introduction

Over the past decades, perovskite solar cells (PSCs), which employ organic-inorganic metal halide hybrid perovskites as light-harvesting materials, have received extensive attention due to their low production cost, solution processing, and good photoelectric characteristics [1–5]. Since the perovskite materials as a photosensitizer were first introduced into dye-sensitized solar cells (DSSCs) and achieved a power conversion efficiency (PCE) of 3.8% in 2009 [6], the PSCs have achieved significant breakthroughs and rapid evolution. Recent technologies can lead to a certified PCE of 25.7%, including device structure and perovskite film quality optimization, interface engineering, and additive engineering [7–10], making PSCs a leading candidate for next-generation photovoltaic technology.

In 2012, the standard solid-state PSCs were assembled for the first time by introducing a solid hole transport material of spiro-OMeTAD to replace liquid electrolytes [11,12]. Since then, the mesoporous structure soon became the most popular geometry to construct PSCs [13,14], as shown in Figure 1a. However, a complicated fabrication process, which involves the deposition of a compact layer followed by a mesoporous TiO₂ layer, is needed for this structure [15]. Meanwhile, a sintering process at a high temperature (usually over 500 °C) is required to remove the organic material in the TiO₂ paste and enhance the crystallinity of the resulting TiO₂ film [16]. These tedious procedures increase the cost of device fabrication and are incompatible with the production of flexible PSCs. In order to overcome the above issues, the planar PSCs were then developed. The long carrier diffusion length and carrier lifetime of commonly used perovskite materials guarantee the effective transport of carriers in this type of solar cell [17,18]. The typical planar PSCs have two different

structures, including the regular n-i-p and inverted p-i-n structures (Figure 1b,c). As for planar PSCs, developing high-quality electron transport layers (ETLs) is crucial to realize high device performance. The ETLs not only can promote the extraction and transport of photo-generated electrons but also block holes to prevent unfavorable charge recombination [4,16]. Currently, many inorganic semiconductors, especially inorganic metal oxides (MOs) such as TiO_2 , ZnO , and SnO_2 , are widely adopted as ETLs in PSCs with planar structure, which is attributed to their low-cost, superb versatility, low-temperature processability, excellent electronic properties, and superior device performance [19–22]. Among them, ZnO is one of the most promising choices owing to its high transparency, high electron mobility, and suitable energy band structure, which can potentially facilitate electron transfer and reduce undesired recombination loss [23,24]. Moreover, ZnO is easy to crystallize, and its intrinsic properties of thin layers can be adjusted simply by doping and manipulating structural composition [25–27]. The compact ZnO used as ETL for planar PSCs cannot only simplify the device fabrication process [28,29] but is also easier to prepare by diverse deposition technologies [27,29–33]. On the other hand, a lower annealing temperature is required for most of the ZnO preparation processes in planar PSCs (usually $<200^\circ\text{C}$), suggesting that it can be produced at a low cost and is suitable for flexible devices [29–34]. However, the high quality of ZnO films should be ensured to achieve more efficient charge transport in planar PSCs. Since the initial introduction of ZnO as ETL into planar PSCs with a PCE of 5.5% [29], continuous enthusiasm and efforts have been devoted to promoting the application of ZnO ETL in PSCs. The performance of planar PSCs based on the compact ZnO ETL has made great progress in recent years; the highest PCE has been boosted to over 21% [35,36]. Although there have been some reviews on the advancement of metal oxide ETLs in PSCs [15,16,37–39], few of them focused on the compact ZnO ETL for planar PSCs systematically.

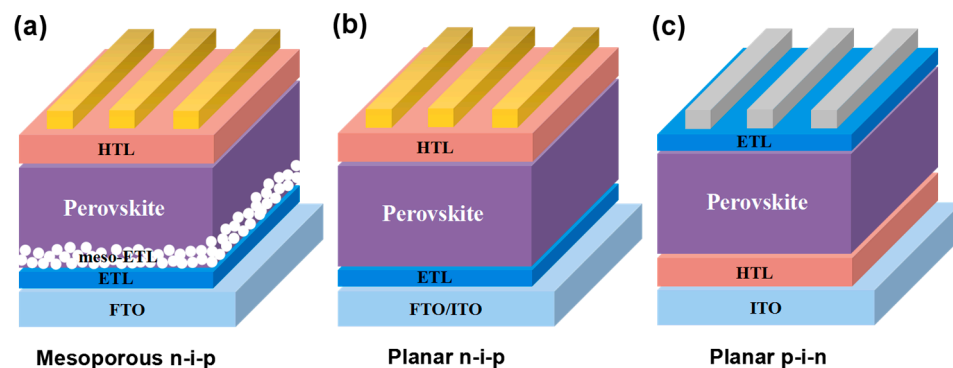


Figure 1. Typical device structures of PSCs: (a) mesoporous n-i-p structure, (b) regular planar structure (n-i-p), and (c) inverted planar structure (p-i-n).

In this review, we first discussed the optical and electronic properties of ZnO , including energy level, mobility, and refractive index. The limitations of ZnO ETL, as well as the effect of optimization strategies, such as doping and surface modification on ZnO , are also covered in our discussion. In addition, the most available fabrication methods of compact ZnO layer were briefly summarized. The recent advances in the application and optimization of ZnO as ETL in planar PSCs are also reviewed. An overall diagram of this review is depicted in Figure 2. Finally, we close our discussion by pointing out the challenges and guidelines for further optimization and design of planar PSCs based on ZnO ETLs.

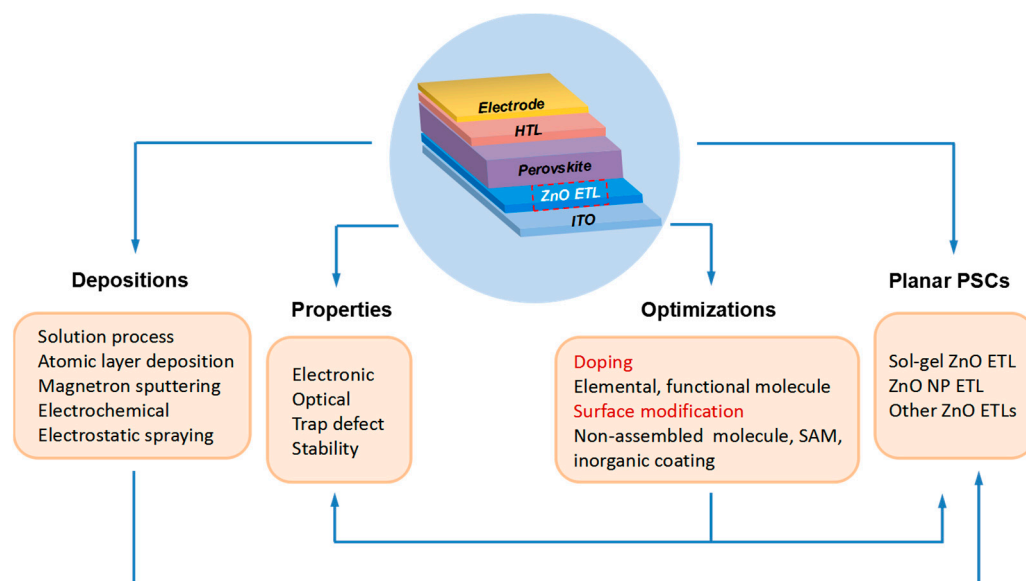


Figure 2. The schematic diagram depicting the review of ZnO as ETL in planar PSCs.

2. ZnO Electron Transport Layer

2.1. Basic Properties of ZnO

In PSCs, the performance of the device heavily relies on the properties of ETLs, especially their optoelectronic property, morphology, and intrinsic defects. As it is adjacent to the perovskite layer, the chemical stability of ETL also has a significant effect on the device's performance.

2.1.1. Optoelectronic Property

ZnO is an inorganic semiconductor with a direct bandgap, and it has a favorable energy level structure for PSCs. The conduction band minimum (CBM) of ZnO locates around -4.17 eV, and its bandgap is 3.2 eV [40,41]. Additionally, it has high transmittance in the range of visible light wavelength as well as a refractive index of about 2.1. The electron mobility of ZnO is $205\text{--}300$ $\text{cm}^2 \cdot \text{V} \cdot \text{s}^{-1}$, and its electron diffusion coefficient is 1.7×10^{-4} $\text{cm}^2 \cdot \text{s}^{-1}$, which is much higher than those of TiO_2 [24,42]. Additionally, ZnO is easy to crystallize and owns good structural tailorability on the nanoscale [34]. A broad range of ZnO-based nanostructures, such as nanoparticles, nanorods, nanowires, nanosheets, nanotubes, and nanobelts, can be fabricated easily at low temperatures [43–48].

2.1.2. Defects

Similar to other semiconductor materials in industrial applications, the intrinsic defects in ZnO have a significant effect on its optical and electrical properties and can evolve into the centers of charge recombination with high density. Generally, there are six kinds of point defects in ZnO, which are oxygen vacancies (V_{O}), Zn vacancies (V_{Zn}), oxygen interstitials (O_{i}), zinc interstitial (Zn_{i}), oxygen antisites (O_{Zn}), and zinc antisites (Zn_{O}) [34]. According to the theoretical calculation and experimental results, V_{O} usually shows the lowest formation energy and hence has the largest concentration in ZnO, and the formation energy of Zn_{i} is also relatively low, and its concentration is high [49,50]. The surface state of ZnO film is another important factor affecting the PSC performance, which can provide recombination pathways by forming a large number of dangling bonds and defects [34]. In addition to being mentioned above, there may be a large lattice mismatch at the interface between ZnO and perovskite when perovskite layers are deposited on the surface of ZnO [51].

2.1.3. Stability

The thermal instability of perovskite on the ZnO surface is one of the crucial problems which has limited the usefulness of ZnO in PSCs. The instability is mainly because the surface of ZnO exhibits basic nature, and the acid-base reaction can happen once perovskite contacts with ZnO [16,51]. Additionally, the hydroxyl groups and chemical residues on the ZnO surface stemming from fabrication processes can accelerate the decomposition of perovskite [48,51], which is another important reason for the instability of devices. Furthermore, ZnO exhibits high photocatalysis activity under ultraviolet (UV) light irradiation, affecting the photostability of PSC devices [34], and the surface hydroxyl groups and remaining chemicals can also cause an aggravation of the photochemical reactions [52].

2.1.4. Regulation of Basic Properties

The problems, such as defect states of ZnO and poor chemical compatibility between ZnO and perovskite, will inevitably affect the device performance. Additionally, the electron mobility and energy level alignment also need to be further improved in the practical application of PSCs [4]. Thus, optimizing ZnO ETL is necessary for high-performance PSCs. Doping is a significantly effective manner to regulate the optoelectronic and physicochemical characteristics of ZnO [16]. This approach not only can passivate defects and reduce the defect state density at the ZnO surface but contributes to a better-aligned energy band between ZnO and perovskite layers owing to the shifted CB of ZnO [4,16]. Moreover, the mobility of ZnO can be enhanced by doping. Therefore, the charge extraction and transport are facilitated, and charge recombination at the interface is suppressed dramatically. Surface modification of ZnO is considered an alternative optimization strategy to doping, which is facile and efficient in tuning the electronic properties and reducing the defect states of the ZnO surface [4,16]. Furthermore, this method can relieve interfacial interactions and weaken the proton transfer reaction of ZnO and perovskite; thus, the stability of perovskite at the interface was remarkably improved.

2.2. Deposition Methods of Compact ZnO ETL

To achieve the highly efficient planar PSCs, the preparation of uniform and compact ZnO thin films without pinholes is essential. The deposition methods of the ZnO layer are diverse. In this section, we simply summarized the principal preparation technologies of ZnO for planar PSCs.

2.2.1. Solution Process

The sol-gel method is one of the most popular methods to deposit the ZnO layer in solution by thermal decomposition of metal-salt precursors, as shown in Figure 3a. To prepare ZnO by this method, a soluble Zn salt or its hydrate dissolved in a suitable solvent is deposited on the substrate by coating [4,34], such as $Zn(NO_3)_2$ or $Zn(CH_3COO)_2$. After that, the as-deposited film is converted to ZnO film by thermal treating. Another commonly employed solution process is the direct synthesis of ZnO nanoparticles (NPs), which decouples the crystallization of ZnO from the forming process of thin films [51,53–55]. The resultant dispersion solution of ZnO NPs is used as a stock solution and can be directly deposited through a variety of coating and printing methods [16]. So far, the solution process is widely applied in high-performance ZnO-based planar PSCs because of the simple operation and good crystallinity of films.

2.2.2. Atomic Layer Deposition (ALD)

As one of the major deposition techniques, ALD can control the growth of thin films finely. Usually, two precursors are used in the ALD process of depositing MO films, one is the metal source, and the other is the oxygen source (oxidant) [56]. One whole preparation flow of ZnO is depicted in Figure 3b, which can be divided into the following steps: (1) exposure of the metal source in the reaction chamber and forms a single molecule film; (2) the excess metal source and the byproducts are purged; (3) exposure of the oxygen

source; and (4) evacuation of the unreacted oxygen source and byproducts [16,56]. By means of the ALD method, high-quality ZnO films with precise thickness control can be produced at low-temperature [4,16]. Nevertheless, this approach is time-consuming and relatively high-cost [4].

2.2.3. Magnetron Sputtering Deposition

As a vacuum coating technology, magnetron sputtering has also been extensively employed to produce ZnO compact layers for planar PSCs. During the working process, a working gas is first injected into a vacuum chamber, and the high energy ion flow can be formed under the action of an electric field [34]. Then, the ionized particles will impact a ZnO ceramic target material, and the sputtered material can deposit and form the ZnO film on a substrate (Figure 3c). The ZnO thin films with high quality can be achieved by optimizing the parameters, including target purity, work gas pressure, gas flow ratio, and radio frequency power [57,58].

2.2.4. Electrochemical Deposition (ED) and Electrostatic Spraying

The compact ZnO layers with high uniformity can be synthesized by the ED method, in which the deposition process is usually performed in a three-electrode cell, and a solution of Zn salt like $\text{Zn}(\text{NO}_3)_2$ with a certain concentration is used as the deposition bath [59]. This method has the advantages of low-temperature preparation, rapid deposition, and controllable deposition thickness [4]. Additionally, the preparation of high-quality ZnO can also be achieved by the electrostatic spraying method. The ordinary course is to spray and deposit the precursor solution of Zn salt onto a substrate under high voltage [34], as shown in Figure 3d. Noteworthy, with this approach, the quality of ZnO layers is significantly dependent on the working voltage, substrate temperature, flow rate of precursor solution and deposition time, etc. [27].

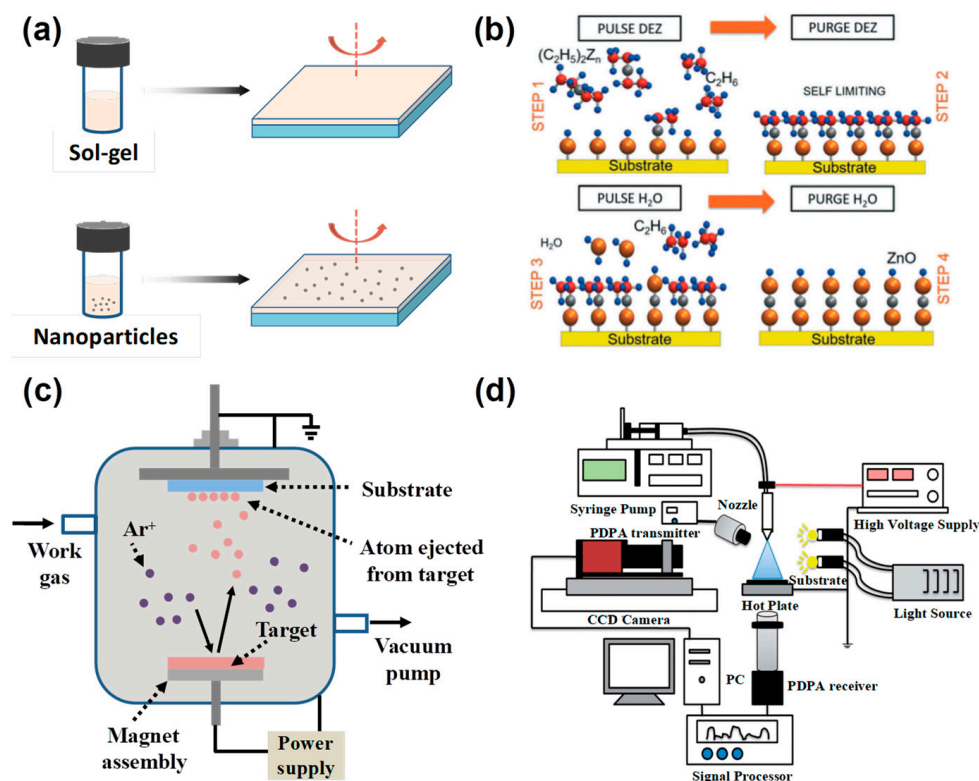


Figure 3. Schematic illustration of the deposition technologies of ZnO thin films: (a) solution process. (b) atomic layer deposition [56]. (c) magnetron sputtering [16]. (d) electrostatic spraying. Reproduced with permission from Ref. [27]. Copyright 2014, Royal Society of Chemistry.

3. Planar PSCs with ZnO ETL

The ZnO films prepared from various deposition methods have become the main candidate of ETL in planar PSCs. The solution process is one of the leading methods to prepare ZnO ETL, including sol-gel ZnO ETL and ZnO NP ETL. Additionally, other deposition methods such as ALD, magnetron sputtering, ED, and electrostatic spraying are also good choices for achieving efficient PSCs. The structure and performance of different ZnO-based planar PSCs are compared and summarized in Table 1.

3.1. PSCs Based on Sol-Gel ZnO ETL

The solution process is the most reported deposition technology of ZnO ETL in planar PSCs, among which the sol-gel method has been widely concerned. In 2014, Lee et al., demonstrated efficient planar PSCs with a sol-gel processed ZnO as ETL, achieving a device efficiency of 8.37% [60]. In their study, a thin layer of organic molecules, [6, 6]-phenyl-C61-butyric acid methyl ester (PCBM) was further introduced on the surface of ZnO to reduce the nonradiative recombination induced by traps at the interface of ZnO as well as in the bulk of perovskite layer, thus improving the PCE to 12.2%. Manspecker et al., obtained MAPbI₃ perovskite on a sol-gel processed ZnO ETL by utilizing a sequential deposition method [61]. They studied the decomposition mechanism of perovskite and revealed the effect of solvent in the perovskite films during annealing. A restricted volume solvent annealing (RVSA) process has been developed to deposit perovskite films on ZnO, resulting in the generation of reproducible PSCs with an efficiency of 13.7%. Zhao et al., also reported the ZnO films achieved by the sol-gel method that was applied as ETLs in planar PSCs, and the device performance of PSCs based on ZnO ETLs made through sol-gel (SG) and hydrolysis-condensation (HC) manners were compared systematically [53]. They found that the HC-ZnO film exhibited a relatively flat surface and higher conductivity; thereby, the PSCs could yield a higher PCE of 12.9%, while a PCE of 10.9% was delivered for the PSCs based on SG-ZnO ETL. In 2017, Zhou et al., reported an aqueous solution-processed route to produce the ZnO ETLs for planar PSCs at low temperatures. An ammine-hydroxo zinc complex solution [62], [Zn(NH₃)_x](OH)₂, was spin-coated on the substrate as the precursor. By utilizing this method, the thermal annealing temperature of ZnO could be reduced to 150 °C, and the prepared ZnO thin films have high transparency and uniformity. Consequently, the PSC with a conventional n-i-p structure showed an efficiency of 10.6% with a high open-circuit voltage of 1.07 V. In addition, by changing the traditional sol-gel method, a simple, effective, scalable approach of combustion synthesis was developed to prepare ZnO ETLs at low temperature for planar PSCs [63], which was comprised of the fuel of acetylacetone and the oxidizer source of Zn(NO₃)₂, respectively. As a comparison, two traditional sol-gel processed ZnO films were also prepared in parallel. By this combustion synthesis process, compact and uniform ZnO films with high crystallinity and fewer impurities were produced, and the ZnO surface can be self-passivated. The resultant PSC devices yielded impressive PCEs close to 20% as well as high stability.

3.2. PSCs Based on ZnO NP ETL

The direct synthesis of ZnO NPs is the most extensively used solution process. The ZnO NP films as the ETL of PSCs were originally studied and realized in 2014 by the Kelly group [30]. They synthesized ZnO NPs by the hydrolysis of Zn(C₂H₃O₂)₂·2H₂O dissolved in methanol, and the NPs could be well dispersed in the mixed solvents of butanol and chloroform without extra surfactants or binders. After that, the compact ZnO NP layers were obtained by spin-coating and used as the ETLs for planar PSCs. The ZnO film was obviously thinner and required no calcination or sintering step. By optimizing the ZnO thickness and perovskite crystal growth, the low-temperature processed PSC devices yielded a promising efficiency of 15.7% and 10.2% on glass and plastic substrates, respectively. Then, they further investigated the effect of CH₃NH₃PbI₃ film thickness and morphology on device efficiency of planar ZnO PSCs [64] and demonstrated that the thermal evaporation of PbI₂ films was a highly reproducible method to fabricate planar

PSCs with very precise control over the perovskite thickness. Based on the ZnO NP ETLs, Hwang et al., fabricated the fully slot-die-coated PSCs using a 3D printed slot-die coater [65]. Consequently, the optimal PCE of 11.96% was produced for the planar PSCs processed at a low temperature, and the results demonstrated the possibility of roll-to-roll mass production of PSCs with ZnO ETL. Zhou et al., developed the ZnO(NP)/CH₃NH₃PbI₃/C planar PSCs without organic hole-transporting layers (HTLs) and metal electrodes at low temperatures [66]. The device architecture and procedure were simple, and the flexible PSCs based on ITO/PEN substrate performed well after 1000 times of bending. In 2016, Song et al., employed commercial ZnO NPs to prepare ZnO thin films used as ETLs for low-temperature planar PSCs [67]. To address the interfacial thermally instability problem between ZnO and perovskite, and further boost the photovoltaic performance of the device, they developed FAPbI₃ as the ZnO-based light absorber and a modified two-step deposition technique to grow the perovskite layer. By optimizing the preparation process of FAPbI₃, the fabricated PSCs yielded the best-performing PCE of up to 16.1%, and the heat resistance of the perovskite layer on ZnO was greatly promoted compared to MA-based perovskite. Subsequently, by utilizing the same ZnO NP ETL, Song et al., confirmed that the triple cation perovskite prepared by a one-step anti-solvent method could be a stable active-layer material for efficient PSCs [68]. An optimum PCE of 18.9% was achieved for the PSC devices with excellent aging resistance and light stability (Figure 4a,b). In 2018, an ultrasonic-assisted method was shown to obtain a ZnO NP solution with high transparency, and the more compact and pinhole-free ZnO NP films were successfully prepared [69]. Meanwhile, a room-temperature aging process of the ZnO layer was carried out to enhance the interfacial stability of ZnO/MAPbI₃ (Figure 4c). Upon optimization of both ZnO and perovskite films, the unencapsulated PSC devices showed high stability even after 45 days of exposure to the air. In addition to regular structure, the ZnO NPs also can be applied in inverted p-i-n PSCs. Bai et al., demonstrated the improved cathode interface using bilayer-structured ETLs of PCBM/ZnO [70], leading to the efficient, stable, and reproducible planar CH₃NH₃PbI_{3-x}Cl_x PSCs with an impressive PCE of up to 15.9%, and the PSC with the large-area of 1 cm² delivered a PCE of 12.3%. Further, a short-time air-aging step has proven to be crucial to promote the performance of PSC devices based on the PCBM/ZnO bilayer [71]. Notably, when implanting ZnO NP ETL in the inverted architecture, the planar PSCs were successfully fabricated with n-type ZnO and p-type NiO_x as NP ETL and NP HTL, respectively, as shown in Figure 4d–e [72]. Compared with the PSCs made with organic layers, the all-metal-oxide charge transport layers enabled the PSC devices had significantly enhanced aging resistance under the ambient conditions, and the maximum PCE of 16.1% was achieved.

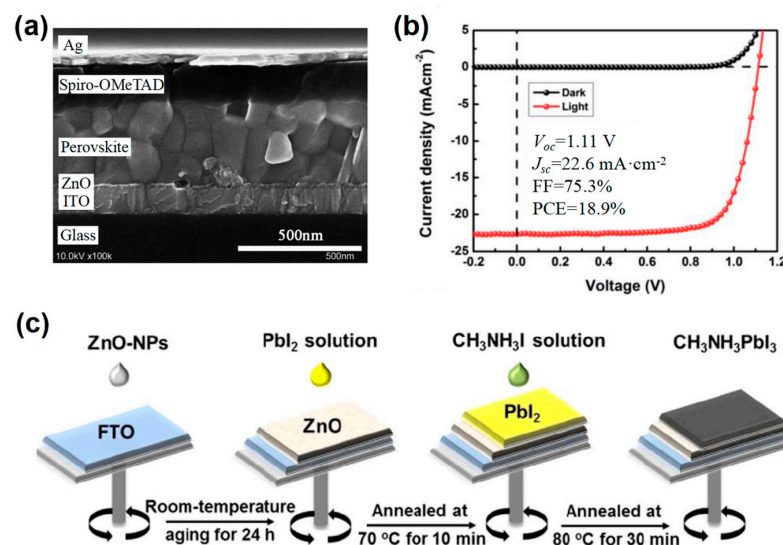


Figure 4. Cont.

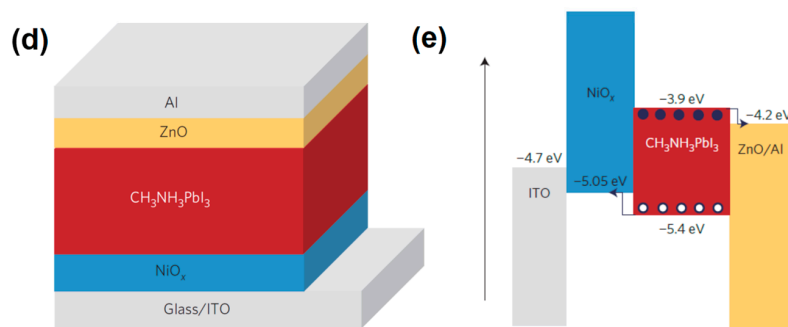


Figure 4. (a) Cross-section SEM picture of the ZnO NP ETL-based triple cation PSC device, and (b) J - V characteristic of the optimum device under illumination and dark, respectively. Reproduced with permission from Ref. [68]. Copyright 2017, Royal Society of Chemistry. (c) Schematic illustration of the preparation process of ZnO/MAPbI₃ by an aging treatment of ZnO NP film and a two-step sequential deposition of perovskite. Reproduced with permission from Ref. [69]. Copyright 2018, Elsevier. (d) Device architecture and (e) energy level of the inverted PSC device with ZnO and NiO_x NPs as ETL and HTL, respectively. Reproduced with permission from Ref. [72]. Copyright 2015, Springer Nature.

3.3. PSCs Based on Other ZnO ETLs

In addition to the solution process, other deposition methods, such as ALD, magnetron sputtering, ED, and electrostatic spraying, have also received extensive attention in ZnO preparation. Lee et al., prepared compact ZnO films as the ETLs of planar PSCs using the ALD technique at a low temperature of 80 °C [73]. Comprehensive studies were performed to understand the effect of the thickness of the ZnO layer on the PSC performance, and the highest PCE of the device could be obtained at a ZnO film thickness of 30 nm. Using this same method, Dong et al., fabricated the planar PSCs by depositing the ZnO films at 70 °C, producing the best device efficiency of 13.1% [74]. It was observed that the compact ZnO film prepared by ALD could promote the formation of CH₃NH₃PbI₃ at room temperature when the perovskite precursor contained chloridion, which was attributed to the reaction between ALD-ZnO and CH₃NH₃Cl. The ALD deposition is also suitable for PSCs with the inverted p-i-n structure. In 2015, Chang et al., adopted a low-temperature ALD technology to grow high-quality ZnO film applied as ETL for inverted planar PSCs [32]. The resulting PSC device revealed a remarkable PCE reaching 16.5% with high reproducibility, which is superior to that of the PSC with ZnO NP ETL (10.8%). Furthermore, the applicability of ALD-ZnO ETL in semitransparent PSCs was also demonstrated by employing Ag nanowires as the top electrode (Figure 5a), and a record-high PCE of 10.8% was achieved. Meanwhile, the Al₂O₃ films prepared by the ALD process were incorporated to serve as the encapsulation layer, and thus the ambient stability of the device was significantly improved.

Magnetron sputtering is a simple and reliable technique. In 2014, Liang et al., reported the magnetron sputtered ZnO film used as the ETL in planar PSCs [75]. The device performance was observed to be insensitive to the thickness of ZnO ETL, which was ascribed to the high electric conductivity of ZnO. As a result, the sputtered ZnO gave a PCE of 13.4% for PSC on a rigid substrate, and the flexible PSC on PET substrates showed a PCE of 8.03%. Tseng et al., investigated the effect of the atmosphere in a sputtering chamber on the formation quality of ZnO [33]. The results demonstrated that the properties, such as the conductivity and band structure of ZnO films, could be tuned by optimizing the ratio of working gases in the process of magnetron sputtering (Figure 5b,c). Finally, an efficiency of up to 15.9% was realized for the regular PSCs when the ZnO ETL was produced under the working gas of pure Ar (Figure 5d), indicating that magnetron sputtering was a splendid technique to fabricate a ZnO layer with controllable properties in planar PSCs. The sputtered ZnO is also a feasible choice in the inverted PSCs. Lai et al., have demonstrated the performance of inverted structured PSCs with a sputtered ZnO ETL [76]. In their research, in order to prevent sputtering damage on perovskite, a C₆₀ interlayer

was introduced between perovskite and ZnO for protection. The resulting optimized PSC exhibited better performance than that based on C_{60}/BCP , as shown in Figure 5e,f.

In 2013, the ED method was employed by Kumar et al., to form a compact ZnO film as ETL [29], and the low-temperature, solution-processed, and flexible PSCs were successfully fabricated by growing ZnO nanorods by chemical bath deposition on electrodeposited ZnO. In addition, Zhang et al., utilized the ED technology for the deposition of the ZnO layer at low temperatures and successfully applied it as ETL in planar PSCs [59]. The effect of the chemical nature and structure of ZnO and TiO_2 ETLs on the formation of $CH_3NH_3PbI_3$ stemming from two different techniques was investigated. The optimum PCE of 15% was yielded for the PSC with an electrodeposited ZnO ETL, a planar architecture, and a one-step method prepared perovskite. Using the electro-spraying method, Mahmood et al., first deposited ZnO and Al-doped ZnO films and studied their application as ETLs for PSCs in 2014 [27]. The quality of ETL films was reported to be controlled by various process parameters, such as the applied voltage, substrate temperature, flow rate, and deposition time. Finally, the Al-doped ZnO thin film fabricated under the optimal parameter conditions delivered a higher PCE of 12.0% for the PSC.

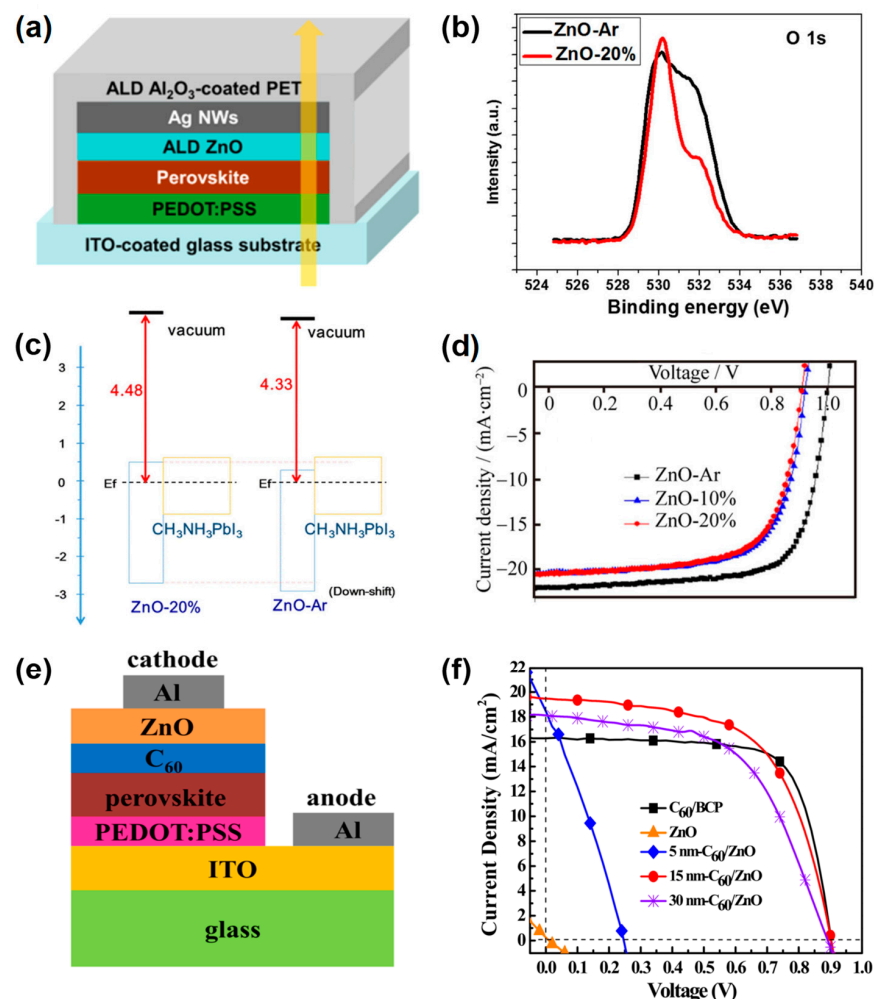


Figure 5. (a) Schematic illustration of semitransparent device architecture based on the ALD processed ZnO ETL [73]. (b) XPS spectra of ZnO films from sputtering under different working gas: pure Ar (ZnO–Ar), 20% O_2 mixture (ZnO–20%) [33], (c) the diagram of energy band for ZnO ETL and perovskite [33], and (d) the J – V characteristics of PSCs based on different ZnO ETLs [33] (e) Device architecture of inverted PSC with sputtered ZnO as ETL, and (f) the J – V curves of PSCs based on different ETLs for comparison. Reproduced with permission from Ref. [76]. Copyright 2015, AIP Publishing.

Table 1. The photovoltaic parameters of planar PSCs based on various ZnO ETLs. The superscript “a” stands for the average value.

	Deposition Method	Device Structure	V_{oc} (V)	J_{sc} (mAcm ⁻²)	FF (%)	PCE (%)	Ref.
Planar	Sol-gel	ITO/ZnO/MAPbI ₃ /PTB7-Th/MoO ₃ /Ag	0.86	14.31	68	8.37	[58]
Planar	Sol-gel	ITO/ZnO/MAPbI ₃ /spiro-OMeTAD/Ag	0.92	20.9	71	13.7	[59]
Planar	Sol-gel	ITO/ZnO/CH ₃ NH ₃ PbI _{3-x} Cl _x /spiro-OMeTAD/Ag	0.93	22.21	52.4	10.9	[51]
Planar	Sol-gel	ITO/ZnO/MAPbI ₃ /spiro-OMeTAD/Ag	1.07	16.81	59	10.6	[62]
Planar	Sol-gel	ITO/ZnO/(Cs _{0.1} FA _{0.9} PbI ₃)/spiro-OMeTAD/Au	1.08	24.67	74.49	19.84	[63]
Planar	Nanoparticle	ITO/ZnO/MAPbI ₃ /spiro-OMeTAD/Ag	1.03	20.4	74.9	15.7	[30]
Planar	Nanoparticle	PET/ITO/ZnO/MAPbI ₃ /spiro-OMeTAD/Ag	1.03	13.4	73.9	10.2	[30]
Planar	Nanoparticle	ITO/ZnO/MAPbI ₃ /P3HT/Ag	0.98	20.38	59.9	11.96	[65]
Planar	Nanoparticle	ZnO/MAPbI ₃ /C	0.54	19.98	54	8.73	[66]
Planar	Nanoparticle	ITO/ZnO/FAPbI ₃ /spiro-OMeTAD/Ag	1.08	20.9	71.3	16.1	[67]
Planar	Nanoparticle	ITO/ZnO/Cs ₆ (MA _{0.17} FA _{0.83}) ₉₄ Pb(I _{0.83} Br _{0.17}) ₃ /spiro-OMeTAD/Ag	1.11	22.6	75.3	18.9	[68]
Planar	Nanoparticle	FTO/ZnO/MAPbI ₃ /spiro-OMeTAD/Au	1.038	19.31	71.09	14.25	[69]
Planar	Nanoparticle	ITO/ZnO/MAPbI ₃ /P3HT/Ag	0.949	18.8	66.1	11.8	[64]
Inverted Planar	Nanoparticle	ITO/PEDOT:PSS/MAPbI _{3-x} Cl _x /PCBM/ZnO/Al	0.97	20.5	80.1	15.9	[70]
Inverted Planar	Nanoparticle	ITO/PEDOT:PSS/MAPbI _{3-x} Cl _{3-x} /PCBM/ZnO/Al	0.98	19.6	74.2	14.2	[71]
Inverted Planar	Nanoparticle	ITO/NiO _x /MAPbI ₃ /ZnO/Al	1.01	21.0	76.0	16.1	[72]
Planar	ALD	ITO/ZnO/MAPbI ₃ /spiro-OMeTAD/MoO ₃ /Ag	0.97 ^a	14.15 ^a	48 ^a	6.59 ^a	[73]
Planar	ALD	FTO/ZnO/MAPbI ₃ /spiro-OMeTAD/Ag	0.97	20.40	66.00	13.10	[74]
Inverted Planar	ALD	ITO/PEDOT:PSS/MAPbI ₃ /ZnO/Ag	1.03	20.75	77.03	16.5	[32]
Planar	Magnetron sputtering	ITO/ZnO/MAPbI ₃ /spiro-OMeTAD/MoO ₃ /Ag	1.04	22.4	57.4	13.4	[75]
Planar	Magnetron sputtering	PET/ITO/ZnO/MAPbI ₃ /spiro-OMeTAD/MoO ₃ /Ag	0.87	18.4	49.7	8.03	[75]
Planar	Magnetron sputtering	ITO/ZnO/MAPbI ₃ /spiro-OMeTAD/Ag	1.00	21.8	72.6	15.9	[33]
Inverted Planar	Magnetron sputtering	ITO/PEDOT:PSS/MAPbI ₃ /C ₆₀ /ZnO/Al	0.91	19.41	62.0	10.93	[76]
Planar	ED	FTO/ZnO/MAPbI ₃ /spiro-OMeTAD/Au	1.02	16.98	51.11	8.90	[29]
Planar	ED	FTO/ZnO/MAPbI ₃ /spiro-OMeTAD/Ag	1.08	20.04	69.47	14.99	[59]
Planar	Electrostatic spraying	FTO/ZnO/MAPbI ₃ /spiro-OMeTAD/Ag	1.01 ^a	16.0 ^a	67.0 ^a	10.8 ^a	[27]

4. The Optimization of ZnO ETLs for Efficient Planar PSCs

To be desirable ETLs and achieve the PSCs with good photovoltaic performance and high stability, further optimizations of ZnO ETL are very necessary. At present, doping and surface modification of ZnO are the two most important approaches to control the optoelectronic and physicochemical properties, reduce the defects and trap states, and improve the interface interaction of ZnO ETL. Here, the recent progress on optimizing ZnO ETL based on doping and surface modification is summarized.

4.1. Doping of ZnO ETL

Elemental doping has been widely used to improve the quality of ZnO ETL. In 2016, Tseng et al., reported the preparation of high-quality, full-coverage Al-doped ZnO (AZO) films (~20 nm) on transparent conductive substrates by magnetron sputtering, and used it as an ETL for the regular planar PSCs [77]. Compared with ZnO films, the AZO showed higher conductivity, better acid resistance, and a more aligned energy band with MAPbI₃, resulting in improved photovoltaic performance. The higher V_{oc} and FF were achieved in the best AZO-based PSC with an efficiency of 17.6%, and the MAPbI₃ films formed onto the AZO had higher thermostability compared with those formed onto the ZnO. Song et al., developed a sol-gel method prepared Mg-doped ZnO (ZMO) used as ETL in planar PSCs [78]. It was found that the photovoltaic performance of the device was strongly dependent on the Mg doping amount, and the champion PCE of 16.5% was

reached for the device with 10% Mg doping. The enhanced PCE originated from the improved optical properties, favorable energy band, efficient electron extraction, and inhibited nonradiative carrier recombination at the ZMO/perovskite interface. More importantly, the $\text{CH}_3\text{NH}_3\text{PbI}_3$ deposited on 10% ZMO thin films demonstrated better heat resistance, and the fabricated PSC device showed improved stability stored in an N_2 atmosphere and under illumination. Then, the lithium (Li) doping low-temperature processed ZnO (L-ZnO) ETL was reported by Mahmud et al., (Figure 6a,b) [79]. After Li doping, the inherent defects in the ZnO films were effectively passivated, and the Fermi energy position of L-ZnO was downshifted by 30 meV. The shifted energy level helped to reduce the electron injection barrier from perovskite to ETL. Consequently, the triple cation (Rb, MA, FA) PSCs incorporating L-ZnO achieved an increased PCE from 14.1% to 16.1% compared to the pure ZnO, which benefited from the superior charge transfer, lowered leakage current, and suppressed nonradiative charge recombination. Azmi et al., prepared the alkali-metal-doped ZnO ETL by dipping ZnO films into various solutions of alkali-metal hydroxide (LiOH, NaOH, and KOH) [80]. The metal doping not only significantly enhanced the electron mobility but also induced a more favorable energy band. Additionally, the surface defects of ZnO films were effectively passivated. Particularly, the deprotonation reaction between perovskite and ZnO was weakened, and the durability of PSCs under ambient air conditions was dramatically raised. A champion device efficiency of 19.9% was yielded for the planar PSC fabricated with K-doped ZnO (ZnO-K), whereas the control device only exhibited a PCE of 16.10%. In addition, similar results could be obtained by Li or Cs doping that was performed by adding either caesium carbonate or lithium acetate into the sol-gel ZnO [81].

On the other hand, there were also some functional molecules that were adopted as dopants of ZnO ETL. Qin et al., reported a new recipe to prepare ZnO by replacing the generally used ethanolamine with polyethylenimine (PEI) in the precursor solution to provide an alkaline environment [82], which could reduce the number of hydroxyl groups on the ZnO surface. With this approach, the thermal decomposition reaction of MA-based perovskite on the ZnO was considerably relieved, as shown in Figure 6c. Additionally, the ZnO prepared from the precursors containing PEI (P-ZnO) was beneficial in inducing the uniform and dense deposition of PCBM on its surface, and block the direct contact between perovskite and P-ZnO layers, hence further improving the thermal stability of perovskite. At last, the PSC with the new ETL combination displayed the best device efficiency of 15.38% (Figure 6d). Recently, Wang et al., employed a strong chelating agent of ethylene diamine tetraacetic acid (EDTA) to develop the EDTA-complexed ZnO (E-ZnO) as the ETL [83]. Compared to pure ZnO, the E-ZnO exhibited more suitable energy levels with perovskite (Figure 6e,f) and improved electron extraction and transport characteristics. Additionally, the E-ZnO chelated with organic ligands of EDTA could effectively mitigate the gradual decomposition of perovskite. Combing the E-ZnO with a new preparation process of perovskite film requiring neither annealing nor antisolvent, the fabricated PSC achieved an impressive PCE of 20.39%, and the long-term stability was significantly improved with retaining 95% of its initial efficiency after 3604 h of exposure in air environment.

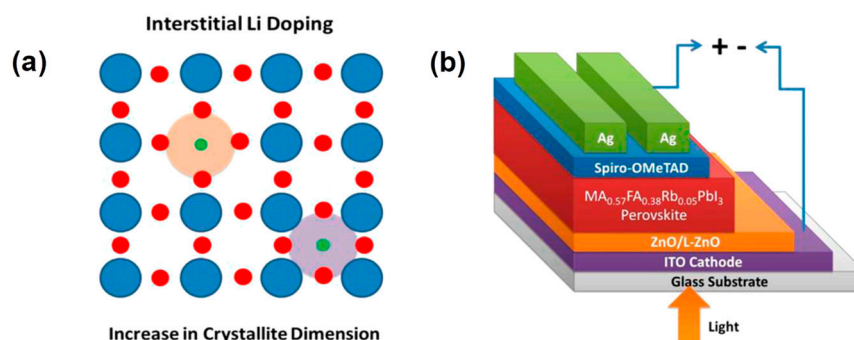


Figure 6. Cont.

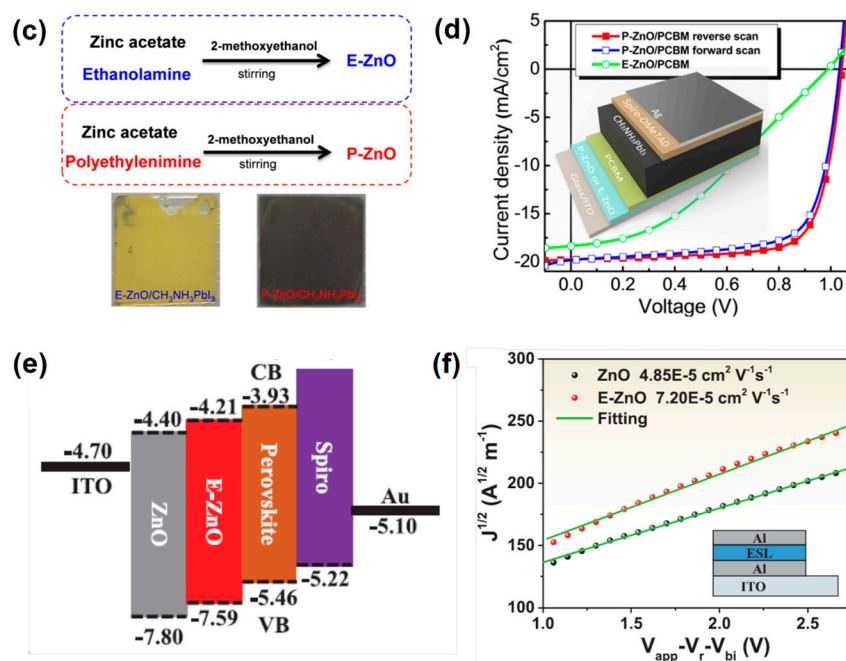


Figure 6. (a) Schematic depicting ZnO lattice structure and interstitial Li doping. In interstitial doping mechanism, Li⁺ passivated the interstitial zinc sites or oxygen vacancies. (b) Schematic illustration of the planar PSC based on the Li-doped ZnO ETL [79] (c) Synthesis steps of E-ZnO and P-ZnO films, and photographs of CH₃NH₃PbI₃ prepared on the different ETLs after thermal annealing at 150 °C for 10 min. (d) *J*–*V* curves of the planar PSCs based on P-ZnO/PCBM ETL and the structure of the PSC device [82] (e) Energy level diagram of the PSC based on ZnO and E-ZnO ETLs, and (f) the electron mobility of ETLs measured by the SCLC method [83].

4.2. Surface Modification of ZnO ETL

Surface modification is another reliable alternative to the doping strategy, mainly serving the purpose of regulating the surface and interface properties of ZnO. So far, non-assembled organic molecules, self-assembled monolayers (SAMs), and inorganic coatings have been broadly employed to modify ZnO ETL for the achievement of high-performance PSCs.

Many non-assembled organic molecules have demonstrated the potential to treat ZnO films for better performance. Cheng et al., found that the thermal treatment could lead to the decomposition of perovskite films deposited on the bare ZnO NP ETL [84]. Therefore, a buffer layer was introduced at the interface of the perovskite and ZnO layers. Notably, the small molecule PCBM can slow down but cannot completely avoid the interfacial reaction of perovskite on ZnO, whereas the polymeric molecular layer of PEI can efficiently avoid direct interaction between ZnO and perovskite. There was no obvious decomposition in perovskite even after an hour of heat treatment at 100 °C, allowing the formation of larger perovskite crystals upon thermal annealing. The PCE of planar PSCs was dramatically raised from 2.9% to 10.2% after the surface modification with PEI. Recently, based on the consideration of eliminating the deprotonation ability of ZnO, Liu et al., introduced methyl ammonium chloride (MACl) on the surface of ZnO NP ETL to improve the surface properties [85]. After the MACl modification and annealing treatment, ZnO could extract H⁺ from MA⁺ and release the CH₃NH₂ gas, thus avoiding the further protonation reaction between ZnO and perovskite. At the same time, Cl would leave on the surface of ZnO and passivate the interfacial defect states. Consequently, the improved efficiency and strengthened durability of planar PSC devices were achieved simultaneously. Additionally, Azmi et al., performed the sulfur passivation on sol-gel ZnO (ZnO-S) ETL by using a simple chemical modification of 1,2-ethanedithiol (EDT), as shown in Figure 7a [86]. With this surface modification, the proton-transfer reaction at the interface of ZnO/perovskite was efficiently prevented, the perovskite growth with larger grain size and higher crystallinity was facilitated, and the

surface defects leading to carrier recombination loss were well passivated. Compared to the pristine ZnO, the PCE significantly increased from 16.51% to 19.65% for the low-temperature planar PSCs based on the ZnO-S ETL, and the unencapsulated device exhibited remarkably improved long-term stability after 40 days of air storage (Figure 7b).

SAM modification was considered a facile and efficient strategy to passivate surface defects and adjust the charging behavior. As a pioneer, Zou et al., developed 3-aminopropanoic acid as the self-assembled molecule (C3-SAM) for the modification of sol-gel ZnO [29]. The deposition of C3-SAM contributed to the improved morphology of $\text{CH}_3\text{NH}_3\text{PbI}_3$ with reduced pinholes and high crystallinity, thus reducing the defect state density of perovskite. Moreover, the interfacial energy level was better aligned because of the formation of a permanent dipole moment. Therefore, a surged PCE from 11.96% to 15.67% was acquired for the planar PSCs. Subsequently, the highly polar molecules of T2CA and JTCA were synthesized by Azmi et al., for the SAM modification on sol-gel ZnO [87]. These SAM molecules enhanced the hydrophobicity of ZnO, resulting in the effective improvement of the formation quality of PbI_2 and final perovskite layers. Meanwhile, the increased electric dipole effect of SAMs enhanced the charge extraction property of PSC devices. A decent PCE of 18.82% was reached for the low-temperature ZnO-based PSC, whereas the pristine device delivered only 15.41%. Recently, Song et al., adopted two thiophene acetic acid-based organic molecules, 2-TA and 3-TA, as SAMs on the ZnO surface for interface modification [88]. The TA-based molecules would interact with ZnO and passivate the trap states on its surface, while the sulfur atom from the thiophene ring could passivate the Pb^{2+} defect of perovskite, as shown in Figure 7c,d. additionally, this TA modification promoted perovskite growth with improved crystallinity and induced a more favorable interfacial energy level alignment. Therefore, the carrier recombination loss caused by defects was reduced, and the interface carrier transport dynamics were improved, contributing to a significantly elevated efficiency from 18.1% to 20.6%. Noteworthily, the perovskite film based on the modified underlayer showed an alleviated thermal decomposition reaction.

In addition to the functional organic molecules, in recent years, several inorganic compounds also have been successfully utilized to modify the ZnO ETL, demonstrating the ability to improve device performance. In 2018, Zheng et al., adopted a thin layer of MgO and a sub-monolayer of protonated ethanolamine (EA) to modify ZnO (Figure 7e) [35]. The charge recombination at the interface of ZnO/perovskite was inhibited by introducing the modification layer of MgO. Additionally, the contact barrier was reduced profited from the protonated EA and hence promoted charge extraction and transport. This modification also nicely resolved the instability issue at the interface. Based on the MgO-EA⁺ modification, the planar PSCs achieved the optimal PCE of 18.3% with improved long-term stability and fully eliminated hysteresis, as shown in Figure 7f. Later, Chen et al., constructed a cascade ZnO-ZnS ETL by sulfurizing the ZnO surface to convert it into ZnS [89]. The sulfide on the surface of ZnO-ZnS could coordinate with Pb^{2+} and generate an electron transport pathway that accelerated electron transfer and reduced charge recombination. Moreover, the ZnS acted as a passivation interlayer to passivate the basic surface of ZnO and avoid the possible proton transfer of perovskite. All these results contributed to enhancing the overall stability of the PSC device and producing a champion PCE of up to 20.7% without appreciable hysteresis. Recently, Pang et al., introduced the PbS quantum dots (QDs) onto ZnO and further deposited the tetrabutylammonium iodide (TBAI) to obtain a new ETL of ZnO/PbS-TBAI for planar PSCs [90]. The non-wetting surface of modified ZnO improved the crystal quality of perovskite, and the more favorable energy level alignment arising from the tunable surface dipole moment of TBAI accelerated electron transfer and transport. Moreover, the decomposition problem of perovskite was completely solved. Based on the PbS QDs modification and optimized TBAI treatment, the ZnO-based PSC achieved an increased PCE from 14.65% to 20.53% with negligible hysteresis, as well as improved stability. In addition, Tavakoli et al., transferred monolayer graphene (MLG) on the surface of ZnO to restrain the possible deprotonation reaction at the interface [91], thereby protecting the perovskite film from decomposition at elevated temperatures. The

introduction of MLG also enhanced the carrier extraction property of ZnO. With the help of MLG modification, a high PCE of 19.81% and excellent operational stability were achieved for the planar PSC device.

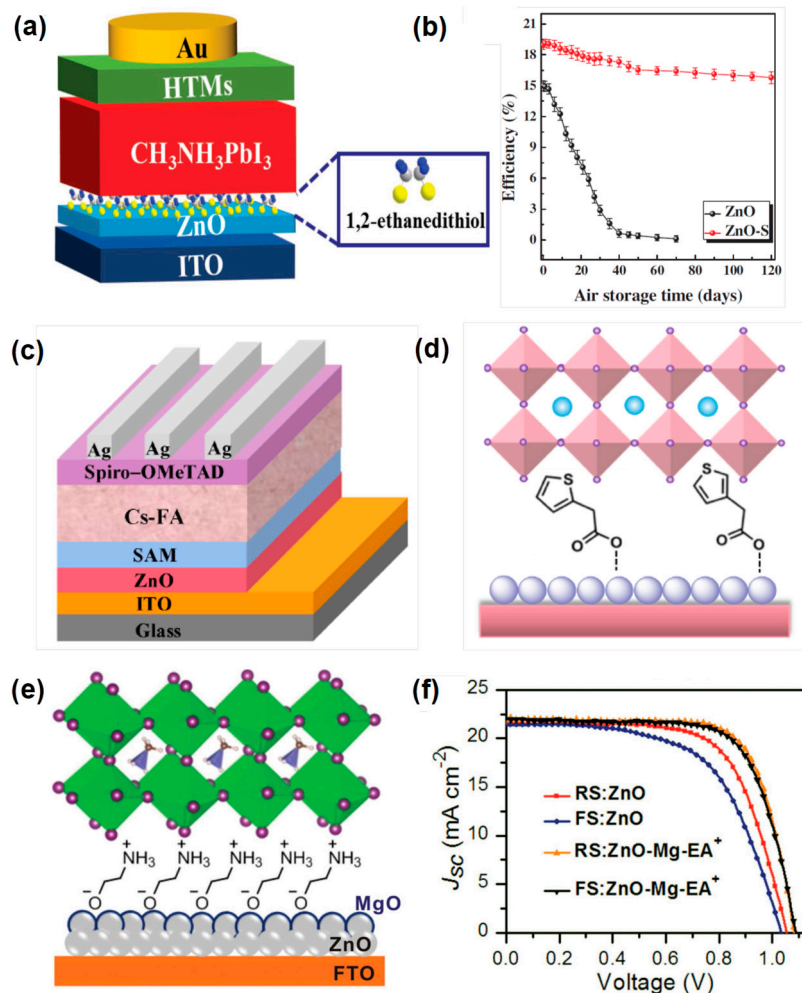


Figure 7. (a) Device structure of PSCs based on the sulfur passivation of ZnO ETL, and (b) the stability test of device exposure to ambient air. Reproduced with permission from Ref. [86]. Copyright 2018, John Wiley and Sons. (c) Device structure of PSCs based on the ZnO ETL with SAM modification, and (d) the schematic diagram of the SAM modification of thiophene acetic acid on ZnO. Reproduced with permission from Ref. [88]. Copyright 2022, Royal Society of Chemistry. (e) Schematic diagram of surface modification of ZnO based on MgO-EA⁺, and (f) *J*-*V* characteristics of the best PSCs. Reproduced with permission from Ref. [35]. Copyright 2018, John Wiley and Sons.

5. Conclusions and Prospective

The ZnO has demonstrated to be a promising candidate as ETL for high-performance planar PSCs, which can significantly simplify the device structure and reduce the processing temperature, thus promoting low-cost and flexible PSCs. Herein, the basic properties of ZnO regarding mobility, energy levels, trap defects as well as chemical stability are clearly introduced to comprehend the relation between ZnO and the resulting PSC device. Moreover, a variety of widely used deposition technologies for preparing ZnO films are presented concisely. At last, we have reviewed the recent advances of ZnO applied as ETLs in efficient planar PSCs. Since ZnO still has some issues, such as mismatched energy bands and insufficient electron mobility, the recent advances in optimization methods on ZnO, including doping and surface modification, are comprehensively summarized and

discussed. Notably, the PCE of planar PSCs based on ZnO has been boosted from 5.0% to over 21% since ZnO as ETL was first introduced into PSCs.

Although great progress has been achieved in the employment of ZnO in planar PSCs, compared with the PSCs based on other MO ETLs, especially the SnO₂ ETL, the performance of planar PSCs using ZnO is still lagging behind. This is primarily due to severe surface recombination, high defect density, and inferior stability of ZnO, hindering its path to becoming an ideal ETL for PSCs with good photovoltaic performance and high stability. Therefore, further optimization of ZnO ETLs is required. On the one hand, more works need to be carried out to finely control the film quality and reduce the defects and surface states of ZnO, making it more efficient in charge transfer by reducing charge recombination and energy loss. In addition to the universal strategies of elemental and functional molecule doping, construction of ternary MOs, and bilayer engineering for optimization of ZnO. According to our latest research [88], surface modification of SAM is regarded as one of the most facile and efficient strategies. The organic molecules with anchoring groups can be adsorbed on the ZnO surface by interacting with ZnO and thus better regulate its surface properties. As a result, the defect state, work function, and surface wettability of ZnO, etc., could be tuned effectively. Considering that perovskite has a large number of surface defects, organic molecules also can introduce additional functional groups like Lewis acid and base to form chemical interaction with the perovskite layer, which is in favor of reducing the trap-assisted recombination loss and facilitating the charge transfer. In the future, the design and synthesis of more novel and efficient SAM molecules with specific functional groups deserve focus. We firmly believe that the ZnO-based planar PSCs with novel SAM modification will achieve further performance breakthroughs.

The instability of perovskite onto ZnO is another important problem that needs to be paid more attention to and is also a major obstacle to their practical application. Due to the effect of thermal instability, the preparation of ZnO-based perovskite is restricted to employing a lower annealing temperature and a shorter annealing time, which is normally inadequate to obtain high-quality perovskite crystals, resulting in decreased PSC performance. Additionally, the interfacial instability can cause performance degeneration and seriously restrict the working stability of the device. Therefore, it is imperative to address the instability problem of ZnO-based PSCs. The introduction of a passivation layer or a buffer layer to obstruct the contact between the ZnO surface and perovskite is an effective method. Based on this strategy, coating ZnO with wide bandgap MOs and decorating ZnO with inorganic QDs all exhibit the great capacity to eliminate the chemical interaction between ZnO and perovskite and passivate the interfacial defects. In particular, in situ constructing hetero-interfaces or hetero-junctions of inorganic semiconductors on ZnO is more likely to become an important means of performance breakthrough. Combined with the improved mobility and optimized energy level benefiting from the inorganic hetero-structures, the device will be promoted toward higher efficiency and stronger stability. Further, we can make more efforts to find out new and robust perovskite materials that are compatible with ZnO ETL. Generally, the FA-based and inorganic perovskite materials are more thermally stable and can be used as stable light absorbers in ZnO-based PSCs. In this case, focusing on various optimization strategies to further enhance the aging resistance and optoelectronic properties of these perovskite materials will be another worthwhile research direction for high-performance ZnO PSCs.

Noteworthy, ZnO ETL is compatible with the fabrication of low-cost and flexible PSCs. Among the commonly utilized approaches for preparing compact ZnO layer, the direct deposition of ZnO by NP solution is a facile process with low energy consumption and high quality. In view of this, the development of colloidal NPs with excellent crystallinity and optoelectronic properties is promising for ZnO-based planar PSCs, and the further optimization of ZnO NP ETL, including elemental doping, organic functional molecule doping, and surface modification may provide an avenue toward high efficiency, large-scale, and flexible PSCs. Overall, in future research, the ZnO will continue to compete with their TiO₂ and SnO₂ analogs for use in PSCs. We believe that the planar PSCs with

ZnO ETL will obtain greater breakthroughs through optimizing and evolving ZnO and perovskite materials and become a competitive candidate for practical application.

Author Contributions: Methodology, J.S. and Z.L.; writing—original draft preparation, C.Q. and Y.W.; writing—review and editing, J.S., W.W. and Z.L.; Visualization, C.Q., Y.W. and J.S. All authors have read and agreed to the published version of the manuscript.

Funding: This research was supported by the Zhejiang Public Welfare Technology Application Research Program (LGJ22B040001), the Innovation Jiaxing-Elite Leading Plan 2020, the Fundamental Research Funds for the Jiaxing University (No. CD70519019, No. CDN70518005), the Jiaxing Public Welfare Research Project (No. 2022AY10003), the Postdoctoral Science Preferential Funding of Zhejiang Province (No. ZJ2022148) and the Zhejiang Provincial Natural Science Foundation of China (No. LQ23E030005).

Institutional Review Board Statement: Not applicable.

Informed Consent Statement: Not applicable.

Data Availability Statement: Not applicable.

Conflicts of Interest: The authors declare no conflict of interest.

References

1. O’regan, B.; Grätzel, M. A low-cost, high-efficiency solar cell based on dye-sensitized colloidal TiO₂ films. *Nature* **1991**, *353*, 737–740. [CrossRef]
2. Gur, I.; Fromer, N.A.; Geier, M.L.; Alivisatos, A.P. Air-stable all-inorganic nanocrystal solar cells processed from solution. *Science* **2005**, *310*, 462–465. [CrossRef]
3. Zeng, G.; Zhang, J.; Chen, X.; Gu, H.; Li, Y.; Li, Y. Breaking 12% efficiency in flexible organic solar cells by using a composite electrode. *Sci. China Chem.* **2019**, *62*, 851–858. [CrossRef]
4. Zhou, Y.; Li, X.; Lin, H. To be higher and stronger-metal oxide electron transport materials for perovskite solar cells. *Small* **2020**, *16*, 1902579. [CrossRef]
5. Ouyang, D.; Huang, Z.; Choy, W.C. Solution-processed metal oxide nanocrystals as carrier transport layers in organic and perovskite solar cells. *Adv. Funct. Mater.* **2019**, *29*, 1804660. [CrossRef]
6. Kojima, A.; Teshima, K.; Shirai, Y.; Miyasaka, T. Organometal halide perovskites as visible-light sensitizers for photovoltaic cells. *J. Am. Chem. Soc.* **2009**, *131*, 6050–6051. [CrossRef]
7. Jeon, N.J.; Noh, J.H.; Kim, Y.C.; Yang, W.S.; Ryu, S.; Seok, S.I. Solvent engineering for high-performance inorganic–organic hybrid perovskite solar cells. *Nat. Mater.* **2014**, *13*, 897–903. [CrossRef]
8. Zhang, M.; Chen, Q.; Xue, R.; Zhan, Y.; Wang, C.; Lai, J.; Yang, J.; Lin, H.; Yao, J.; Li, Y.; et al. Reconfiguration of interfacial energy band structure for high-performance inverted structure perovskite solar cells. *Nat. Commun.* **2019**, *10*, 4593. [CrossRef]
9. Jiang, Q.; Ni, Z.; Xu, G.; Lin, Y.; Rudd, P.N.; Xue, R.; Li, Y.; Li, Y.; Gao, Y.; Huang, J. Interfacial molecular doping of metal halide perovskites for highly efficient solar cells. *Adv. Mater.* **2020**, *32*, 2001581. [CrossRef]
10. National Renewable Energy Laboratory 2022, Best Research Cell Efficiencies. Available online: <https://www.nrel.gov/pv/assets/pdfs/best-research-cell-efficiencies.pdf>. (accessed on 30 September 2022).
11. Im, J.H.; Lee, C.R.; Lee, J.W.; Park, S.W.; Park, N.G. 6.5% efficient perovskite quantum-dot-sensitized solar cell. *Nanoscale* **2011**, *3*, 4088–4093. [CrossRef]
12. Kim, H.S.; Lee, C.R.; Im, J.H.; Lee, K.B.; Moehl, T.; Marchioro, A.; Moon, S.J.; Humphry-Baker, R.; Yum, J.H.; Moser, J.E.; et al. Lead iodide perovskite sensitized all-solid-state submicron thin film mesoscopic solar cell with efficiency exceeding 9%. *Sci. Rep.* **2012**, *2*, 591. [CrossRef]
13. Burschka, J.; Pellet, N.; Moon, S.J.; Humphry-Baker, R.; Gao, P.; Nazeeruddin, M.K.; Grätzel, M. Sequential deposition as a route to high-performance perovskite-sensitized solar cells. *Nature* **2013**, *499*, 316–319. [CrossRef]
14. Shaikh, S.F.; Kwon, H.C.; Yang, W.; Mane, R.S.; Moon, J. Performance enhancement of mesoporous TiO₂-based perovskite solar cells by ZnS ultrathin-interfacial modification layer. *J. Alloy. Compd.* **2018**, *738*, 405–414. [CrossRef]
15. Shin, S.S.; Lee, S.J.; Seok, S.I. Metal oxide charge transport layers for efficient and stable perovskite solar cells. *Adv. Funct. Mater.* **2019**, *29*, 1900455. [CrossRef]
16. Song, J.X.; Yin, X.X.; Li, Z.F.; Li, Y.W. Low-temperature-processed metal oxide electron transport layers for efficient planar perovskite solar cells. *Rare Met.* **2021**, *40*, 2730–2746. [CrossRef]
17. Stranks, S.D.; Eperon, G.E.; Grancini, G.; Menelaou, C.; Alcocer, M.J.P.; Leijtens, T.; Herz, L.M.; Petrozza, A.; Snaith, H.J. Electron-hole diffusion lengths exceeding 1 micrometer in an organometal trihalide perovskite absorber. *Science* **2013**, *342*, 341–344. [CrossRef]
18. Liu, M.; Johnston, M.B.; Snaith, H.J. Efficient planar heterojunction perovskite solar cells by vapour deposition. *Nature* **2013**, *501*, 395–398. [CrossRef]

19. Docampo, P.; Ball, J.M.; Darwich, M.; Eperon, G.E.; Snaith, H.J. Efficient organometal trihalide perovskite planar-heterojunction solar cells on flexible polymer substrates. *Nat. Commun.* **2013**, *4*, 2761. [[CrossRef](#)]
20. Zhou, H.; Chen, Q.; Li, G.; Luo, S.; Song, T.B.; Duan, H.S.; Hong, Z.; You, J.; Liu, Y.; Yang, Y. Interface engineering of highly efficient perovskite solar cells. *Science* **2014**, *345*, 542–546. [[CrossRef](#)]
21. Song, J.; Zheng, E.; Bian, J.; Wang, X.F.; Tian, W.; Sanehira, Y.; Miyasaka, T. Low-temperature SnO₂-based electron selective contact for efficient and stable perovskite solar cells. *J. Mater. Chem. A* **2015**, *3*, 10837–10844. [[CrossRef](#)]
22. Ke, W.; Fang, G.; Liu, Q.; Xiong, L.; Qin, P.; Tao, H.; Wang, J.; Lei, H.; Li, B.; Wan, J.; et al. Low-temperature solution-processed tin oxide as an alternative electron transporting layer for efficient perovskite solar cells. *J. Am. Chem. Soc.* **2015**, *137*, 6730–6733. [[CrossRef](#)]
23. Wang, Z.L. Zinc oxide nanostructures: Growth, properties and applications. *J. Phys. Condens. Matter* **2004**, *16*, R829. [[CrossRef](#)]
24. Zhang, Q.; Dandeneau, C.S.; Zhou, X.; Cao, G. ZnO nanostructures for dye-sensitized solar cells. *Adv. Mater.* **2009**, *21*, 4087–4108. [[CrossRef](#)]
25. Dong, J.; Zhao, Y.; Shi, J.; Wei, H.; Xiao, J.; Xu, X.; Luo, J.; Xu, J.; Li, D.; Luo, Y.; et al. Impressive enhancement in the cell performance of ZnO nanorod-based perovskite solar cells with Al-doped ZnO interfacial modification. *Chem. Commun.* **2014**, *50*, 13381–13384. [[CrossRef](#)]
26. Zhang, J.; Barboux, P.; Pauporté, T. Electrochemical design of nanostructured ZnO charge carrier layers for efficient solid-state perovskite-sensitized solar cells. *Adv. Energy Mater.* **2014**, *4*, 1400932. [[CrossRef](#)]
27. Mahmood, K.; Swain, B.S.; Jung, H.S. Controlling the surface nanostructure of ZnO and Al-doped ZnO thin films using electrostatic spraying for their application in 12% efficient perovskite solar cells. *Nanoscale* **2014**, *6*, 9127–9138. [[CrossRef](#)]
28. Son, D.Y.; Im, J.H.; Kim, H.S.; Park, N.G. 11% efficient perovskite solar cell based on ZnO nanorods: An effective charge collection system. *J. Phys. Chem.* **2014**, *118*, 16567–16573. [[CrossRef](#)]
29. Kumar, M.H.; Yantara, N.; Dharani, S.; Graetzel, M.; Mhaisalkar, S.; Boix, P.P.; Mathews, N. Flexible, low-temperature, solution processed ZnO-based perovskite solid state solar cells. *Chem. Commun.* **2013**, *49*, 11089–11091. [[CrossRef](#)]
30. Liu, D.; Kelly, T.L. Perovskite solar cells with a planar heterojunction structure prepared using room-temperature solution processing techniques. *Nat. Photonics* **2014**, *8*, 133–138. [[CrossRef](#)]
31. Zuo, L.; Gu, Z.; Ye, T.; Fu, W.; Wu, G.; Li, H.; Chen, H. Enhanced photovoltaic performance of CH₃NH₃PbI₃ perovskite solar cells through interfacial engineering using self-assembling monolayer. *J. Am. Chem. Soc.* **2015**, *137*, 2674–2679. [[CrossRef](#)]
32. Chang, C.Y.; Lee, K.T.; Huang, W.K.; Siao, H.Y.; Chang, Y.C. High-performance, air-stable, low-temperature processed semitransparent perovskite solar cells enabled by atomic layer deposition. *Chem. Mater.* **2015**, *27*, 5122–5130. [[CrossRef](#)]
33. Tseng, Z.L.; Chiang, C.H.; Wu, C.G. Surface engineering of ZnO thin film for high efficiency planar perovskite solar cells. *Sci. Rep.* **2015**, *5*, 13211. [[CrossRef](#)]
34. Zhang, P.; Wu, J.; Zhang, T.; Wang, Y.; Liu, D.; Chen, H.; Ji, L.; Liu, C.; Ahmad, W.; Chen, Z.D.; et al. Perovskite solar cells with ZnO electron-transporting materials. *Adv. Mater.* **2018**, *30*, 1703737. [[CrossRef](#)]
35. Cao, J.; Wu, B.; Chen, R.; Wu, Y.; Hui, Y.; Mao, B.W.; Zheng, N. Efficient, Hysteresis-Free, and Stable Perovskite Solar Cells with ZnO as Electron-Transport Layer: Effect of Surface Passivation. *Adv. Mater.* **2018**, *30*, 1705596. [[CrossRef](#)]
36. Schutt, K.; Nayak, P.K.; Ramadan, A.J.; Wenger, B.; Lin, Y.H.; Snaith, H.J. Overcoming zinc oxide interface instability with a methylammonium-free perovskite for high-performance solar cells. *Adv. Funct. Mater.* **2019**, *29*, 1900466. [[CrossRef](#)]
37. Singh, T.; Singh, J.; Miyasaka, T. Role of metal oxide electron-transport layer modification on the stability of high performing perovskite solar cells. *ChemSusChem* **2016**, *9*, 2559–2566. [[CrossRef](#)]
38. Haque, M.A.; Sheikh, A.D.; Guan, X.; Wu, T. Metal oxides as efficient charge transporters in perovskite solar cells. *Adv. Energy Mater.* **2017**, *7*, 1602803. [[CrossRef](#)]
39. Jiang, Q.; Zhang, X.; You, J. SnO₂: A wonderful electron transport layer for perovskite solar cells. *Small* **2018**, *14*, 1801154. [[CrossRef](#)]
40. Xue, S.W.; Zu, X.T.; Zhou, W.L.; Deng, H.X.; Xiang, X.; Zhang, L.; Deng, H. Effects of post-thermal annealing on the optical constants of ZnO thin film. *J. Alloys Compd.* **2008**, *448*, 21–26. [[CrossRef](#)]
41. Srikant, V.; Clarke, D.R. On the optical band gap of zinc oxide. *J. Appl. Phys.* **1998**, *83*, 5447–5451. [[CrossRef](#)]
42. Look, D.C.; Reynolds, D.C.; Sizelove, J.R.; Jones, R.L.; Litton, C.W.; Cantwell, G.; Harsch, W.C. Electrical properties of bulk ZnO. *Solid State Commun.* **1998**, *105*, 399–401. [[CrossRef](#)]
43. Pacholski, C.; Kornowski, A.; Weller, H. Self-assembly of ZnO: From nanodots to nanorods. *Angew. Chem. Int. Ed.* **2002**, *41*, 1188–1191. [[CrossRef](#)]
44. Wang, X.; Summers, C.J.; Wang, Z.L. Large-scale hexagonal-patterned growth of aligned ZnO nanorods for nano-optoelectronics and nanosensor arrays. *Nano Lett.* **2004**, *4*, 423–426. [[CrossRef](#)]
45. Kong, Y.C.; Yu, D.P.; Zhang, B.; Fang, W.; Feng, S.Q. Ultraviolet-emitting ZnO nanowires synthesized by a physical vapor deposition approach. *Appl. Phys. Lett.* **2001**, *78*, 407–409. [[CrossRef](#)]
46. Sun, Y.; Fuge, G.M.; Fox, N.A.; Riley, D.J.; Ashfold, M.N. Synthesis of aligned arrays of ultrathin ZnO nanotubes on a Si wafer coated with a thin ZnO film. *Adv. Mater.* **2005**, *17*, 2477–2481. [[CrossRef](#)]
47. Ronning, C.; Gao, P.X.; Ding, Y.; Wang, Z.L.; Schwen, D. Manganese-doped ZnO nanobelts for spintronics. *Appl. Phys. Lett.* **2004**, *84*, 783–785. [[CrossRef](#)]

48. Luo, J.; Wang, Y.; Zhang, Q. Progress in perovskite solar cells based on ZnO nanostructures. *Sol. Energy* **2018**, *163*, 289–306. [[CrossRef](#)]
49. Oba, F.; Nishitani, S.R.; Isotani, S.; Adachi, H.; Tanaka, I. Energetics of native defects in ZnO. *J. Appl. Phys.* **2001**, *90*, 824–828. [[CrossRef](#)]
50. Kohan, A.F.; Ceder, G.; Morgan, D.; Van de Walle, C.G. First-principles study of native point defects in ZnO. *Phys. Rev.* **2000**, *61*, 15019. [[CrossRef](#)]
51. Yang, J.; Siempelkamp, B.D.; Mosconi, E.; De Angelis, F.; Kelly, T.L. Origin of the thermal instability in CH₃NH₃PbI₃ thin films deposited on ZnO. *Chem. Mater.* **2015**, *27*, 4229–4236. [[CrossRef](#)]
52. Zhang, P.; Wu, J.; Wang, Y.; Sarvari, H.; Liu, D.; Chen, Z.D.; Li, S. Enhanced efficiency and environmental stability of planar perovskite solar cells by suppressing photocatalytic decomposition. *J. Mater. Chem.* **2017**, *5*, 17368–17378. [[CrossRef](#)]
53. Zhao, Y.H.; Zhang, K.C.; Wang, Z.W.; Huang, P.; Zhu, K.; Li, Z.D.; Li, D.H.; Yuan, L.G.; Zhou, Y.; Song, B. Comprehensive study of sol-gel versus hydrolysis-condensation methods to prepare ZnO films: Electron transport layers in perovskite solar cells. *ACS Appl. Mater. Interfaces* **2017**, *9*, 26234–26241. [[CrossRef](#)] [[PubMed](#)]
54. Song, J.; Bian, J.; Zheng, E.; Wang, X.F.; Tian, W.; Miyasaka, T. Efficient and environmentally stable perovskite solar cells based on ZnO electron collection layer. *Chem. Lett.* **2015**, *44*, 610–612. [[CrossRef](#)]
55. Sun, Y.; Seo, J.H.; Takacs, C.J.; Seifert, J.; Heeger, A.J. Inverted polymer solar cells integrated with a low-temperature-annealed sol-gel-derived ZnO film as an electron transport layer. *Adv. Mater.* **2011**, *23*, 1679–1683. [[CrossRef](#)]
56. Oviroh, P.O.; Akbarzadeh, R.; Pan, D.; Coetzee, R.A.M.; Jen, T.C. New development of atomic layer deposition: Processes, methods and applications. *Sci. Technol. Adv. Mater.* **2019**, *20*, 465–496. [[CrossRef](#)] [[PubMed](#)]
57. Carcia, P.F.; McLean, R.S.; Reilly, M.H.; Nunes, G., Jr. Transparent ZnO thin-film transistor fabricated by rf magnetron sputtering. *Appl. Phys. Lett.* **2003**, *82*, 1117–1119. [[CrossRef](#)]
58. Kim, K.H.; Park, K.C.; Ma, D.Y. Structural, electrical and optical properties of aluminum doped zinc oxide films prepared by radio frequency magnetron sputtering. *J. Appl. Phys.* **1997**, *81*, 7764–7772. [[CrossRef](#)]
59. Zhang, J.; Pauporté, T. Effects of oxide contact layer on the preparation and properties of CH₃NH₃PbI₃ for perovskite solar cell application. *J. Phys. Chem.* **2015**, *119*, 14919–14928. [[CrossRef](#)]
60. Kim, J.; Kim, G.; Kim, T.K.; Kwon, S.; Back, H.; Lee, J.; Lee, H.S.; Kang, H.; Lee, K. Efficient planar-heterojunction perovskite solar cells achieved via interfacial modification of a sol-gel ZnO electron collection layer. *J. Mater. Chem. A* **2014**, *2*, 17291–17296. [[CrossRef](#)]
61. Manspeaker, C.; Scruggs, P.; Preiss, J.; Lyashenko, D.A.; Zakhidov, A.A. Reliable annealing of CH₃NH₃PbI₃ films deposited on ZnO. *J. Phys. Chem.* **2016**, *120*, 6377–6382. [[CrossRef](#)]
62. Zhou, J.; Meng, X.; Zhang, X.; Tao, X.; Zhang, Z.; Hu, J.; Wang, C.; Li, Y.; Yang, S. Low-temperature aqueous solution processed ZnO as an electron transporting layer for efficient perovskite solar cells. *Mater. Chem. Front.* **2017**, *1*, 802–806. [[CrossRef](#)]
63. Zheng, D.; Wang, G.; Huang, W.; Wang, B.; Ke, W.; Logsdon, J.L.; Wang, H.; Wang, Z.; Zhu, W.; Yu, J.; et al. Combustion synthesized zinc oxide electron-transport layers for efficient and stable perovskite solar cells. *Adv. Funct. Mater.* **2019**, *29*, 1900265. [[CrossRef](#)]
64. Liu, D.; Gangishetty, M.K.; Kelly, T.L. Effect of CH₃NH₃PbI₃ thickness on device efficiency in planar heterojunction perovskite solar cells. *J. Mater. Chem.* **2014**, *2*, 19873–19881. [[CrossRef](#)]
65. Hwang, K.; Jung, Y.S.; Heo, Y.J.; Scholes, F.H.; Watkins, S.E.; Subbiah, J.; Jones, D.J.; Kim, D.Y.; Vak, D. Toward large scale roll-to-roll production of fully printed perovskite solar cells. *Adv. Mater.* **2015**, *27*, 1241–1247. [[CrossRef](#)]
66. Zhou, H.; Shi, Y.; Wang, K.; Dong, Q.; Bai, X.; Xing, Y.; Du, Y.; Ma, T. Low-temperature processed and carbon-based ZnO/CH₃NH₃PbI₃/C planar heterojunction perovskite solar cells. *J. Phys. Chem.* **2015**, *119*, 4600–4605. [[CrossRef](#)]
67. Song, J.; Hu, W.; Wang, X.F.; Chen, G.; Tian, W.; Miyasaka, T. HC(NH₂)₂PbI₃ as a thermally stable absorber for efficient ZnO-based perovskite solar cells. *J. Mater. Chem.* **2016**, *4*, 8435–8443. [[CrossRef](#)]
68. Song, J.; Liu, L.; Wang, X.F.; Chen, G.; Tian, W.; Miyasaka, T. Highly efficient and stable low-temperature processed ZnO solar cells with triple cation perovskite absorber. *J. Mater. Chem.* **2017**, *5*, 13439–13447. [[CrossRef](#)]
69. Guo, Y.; Kang, L.; Zhu, M.; Zhang, Y.; Li, X.; Xu, P. A strategy toward air-stable and high-performance ZnO-based perovskite solar cells fabricated under ambient conditions. *Chem. Eng. J.* **2018**, *336*, 732–740. [[CrossRef](#)]
70. Bai, S.; Wu, Z.; Wu, X.; Jin, Y.; Zhao, N.; Chen, Z.; Mei, Q.; Wang, X.; Ye, Z.; Song, T.; et al. High-performance planar heterojunction perovskite solar cells: Preserving long charge carrier diffusion lengths and interfacial engineering. *Nano Res.* **2014**, *7*, 1749–1758. [[CrossRef](#)]
71. Qiu, W.; Buffiere, M.; Brammertz, G.; Paetzold, U.W.; Froyen, L.; Heremans, P.; Cheyns, D. High efficiency perovskite solar cells using a PCBM/ZnO double electron transport layer and a short air-aging step. *Org. Electron.* **2015**, *26*, 30–35. [[CrossRef](#)]
72. You, J.; Meng, L.; Song, T.B.; Guo, T.F.; Yang, Y.M.; Chang, W.H.; Hong, Z.; Chen, H.; Zhou, H.; Chen, Q.; et al. Improved air stability of perovskite solar cells via solution-processed metal oxide transport layers. *Nat. Nanotechnol.* **2016**, *11*, 75–81. [[CrossRef](#)]
73. Lee, K.M.; Chang, S.H.; Wang, K.H.; Chang, C.M.; Cheng, H.M.; Kei, C.C.; Tseng, Z.L.; Wu, C.G. Thickness effects of ZnO thin film on the performance of tri-iodide perovskite absorber based photovoltaics. *Sol. Energy* **2015**, *120*, 117–122. [[CrossRef](#)]
74. Dong, X.; Hu, H.; Lin, B.; Ding, J.; Yuan, N. The effect of ALD-ZnO layers on the formation of CH₃NH₃PbI₃ with different perovskite precursors and sintering temperatures. *Chem. Commun.* **2014**, *50*, 14405–14408. [[CrossRef](#)] [[PubMed](#)]

75. Liang, L.; Huang, Z.; Cai, L.; Chen, W.; Wang, B.; Chen, K.; Bai, H.; Tian, Q.; Fan, B. Magnetron sputtered zinc oxide nanorods as thickness-insensitive cathode interlayer for perovskite planar-heterojunction solar cells. *ACS Appl. Mater. Interfaces* **2014**, *6*, 20585–20589. [[CrossRef](#)]
76. Lai, W.C.; Lin, K.W.; Guo, T.F.; Chen, P.; Wang, Y.T. Conversion efficiency improvement of inverted CH₃NH₃PbI₃ perovskite solar cells with room temperature sputtered ZnO by adding the C₆₀ interlayer. *Appl. Phys. Lett.* **2015**, *107*, 253301. [[CrossRef](#)]
77. Tseng, Z.L.; Chiang, C.H.; Chang, S.H.; Wu, C.G. Surface engineering of ZnO electron transporting layer via Al doping for high efficiency planar perovskite solar cells. *Nano Energy* **2016**, *28*, 311–318. [[CrossRef](#)]
78. Song, J.; Zheng, E.; Liu, L.; Wang, X.F.; Chen, G.; Tian, W.; Miyasaka, T. Magnesium-doped Zinc Oxide as Electron Selective Contact Layers for Efficient Perovskite Solar Cells. *ChemSusChem* **2016**, *9*, 2640–2647. [[CrossRef](#)]
79. Mahmud, M.A.; Elumalai, N.K.; Upama, M.B.; Wang, D.; Soufiani, A.M.; Wright, M.; Xu, C.; Haque, F.; Uddin, A. Solution-Processed Lithium-Doped ZnO Electron Transport Layer for Efficient Triple Cation (Rb, MA, FA) Perovskite Solar Cells. *ACS Appl. Mater. Interfaces* **2017**, *9*, 33841–33854. [[CrossRef](#)]
80. Azmi, R.; Hwang, S.; Yin, W.; Kim, T.W.; Ahn, T.K.; Jang, S.Y. High efficiency low-temperature processed perovskite solar cells integrated with alkali metal doped ZnO electron transport layers. *ACS Energy Lett.* **2018**, *3*, 1241–1246. [[CrossRef](#)]
81. An, Q.; Fassl, P.; Hofstetter, Y.J.; Becker-Koch, D.; Bausch, A.; Hopkinson, P.E.; Vaynzof, Y. High performance planar perovskite solar cells by ZnO electron transport layer engineering. *Nano Energy* **2017**, *39*, 400–408. [[CrossRef](#)]
82. Qin, F.; Meng, W.; Fan, J.; Ge, C.; Luo, B.; Ge, R.; Hu, L.; Jiang, F.; Liu, T.; Jiang, Y.; et al. Enhanced Thermochemical Stability of CH₃NH₃PbI₃ Perovskite Films on Zinc Oxides via New Precursors and Surface Engineering. *ACS Appl. Mater. Interfaces* **2017**, *9*, 26045–26051. [[CrossRef](#)] [[PubMed](#)]
83. Wang, Z.; Zhu, X.; Feng, J.; Wang, C.; Zhang, C.; Ren, X.; Priya, S.; Liu, S.F.; Yang, D. Antisolvent- and Annealing-Free Deposition for Highly Stable Efficient Perovskite Solar Cells via Modified ZnO. *Adv. Sci.* **2021**, *8*, 2002860. [[CrossRef](#)] [[PubMed](#)]
84. Cheng, Y.; Yang, Q.D.; Xiao, J.; Xue, Q.; Li, H.W.; Guan, Z.; Yip, H.L.; Tsang, S.W. Decomposition of Organometal Halide Perovskite Films on Zinc Oxide Nanoparticles. *ACS Appl. Mater. Interfaces* **2015**, *7*, 19986–19993. [[CrossRef](#)] [[PubMed](#)]
85. Liu, C.; Wu, W.; Zhang, D.; Li, Z.; Ren, G.; Han, W.; Guo, W. Effective stability enhancement in ZnO-based perovskite solar cells by MAcl modification. *J. Mater. Chem.* **2021**, *9*, 12161–12168. [[CrossRef](#)]
86. Azmi, R.; Lee, C.L.; Jung, I.H.; Jang, S.Y. Simultaneous Improvement in Efficiency and Stability of Low-Temperature-Processed Perovskite Solar Cells by Interfacial Control. *Adv. Energy Mater.* **2018**, *8*, 1702934. [[CrossRef](#)]
87. Azmi, R.; Hadmojo, W.T.; Sinaga, S.; Lee, C.L.; Yoon, S.C.; Jung, I.H.; Jang, S.Y. High-Efficiency Low-Temperature ZnO Based Perovskite Solar Cells Based on Highly Polar, Nonwetting Self-Assembled Molecular Layers. *Adv. Energy Mater.* **2018**, *8*, 1701683. [[CrossRef](#)]
88. Wu, Y.; Song, J.; Wu, X.; Qiu, C.; Yin, X.; Hu, L.; Su, Z.; Jin, Y.; Chen, J.; Li, Z. Highly efficient and stable ZnO-based perovskite solar cells enabled by a self-assembled monolayer as the interface linker. *Chem. Commun.* **2022**, *58*, 9266–9269. [[CrossRef](#)]
89. Chen, R.; Cao, J.; Duan, Y.; Hui, Y.; Chuong, T.T.; Ou, D.; Han, F.; Cheng, F.; Huang, X.; Wu, B.; et al. High-Efficiency, Hysteresis-Less, UV-Stable Perovskite Solar Cells with Cascade ZnO-ZnS Electron Transport Layer. *J. Am. Chem. Soc.* **2019**, *141*, 541–547. [[CrossRef](#)]
90. Pang, Z.; Yang, S.; Sun, Y.; He, L.; Wang, F.; Fan, L.; Chi, S.; Sun, X.; Yang, L.; Yang, J. Hydrophobic PbS QDs layer decorated ZnO electron transport layer to boost photovoltaic performance of perovskite solar cells. *Chem. Eng. J.* **2022**, *439*, 135701. [[CrossRef](#)]
91. Tavakoli, M.M.; Tavakoli, R.; Yadav, P.; Kong, J. A graphene/ZnO electron transfer layer together with perovskite passivation enables highly efficient and stable perovskite solar cells. *J. Mater. Chem.* **2019**, *7*, 679–686. [[CrossRef](#)]